Random transparency targets for modulation transfer function measurement in the visible and infrared regions

Arnold Daniels, MEMBER SPIE
Glenn D. Boreman, MEMBER SPIE
Alfred D. Ducharme
University of Central Florida
Department of Electrical Engineering
Center for Research and Education in Optics and Lasers (CREOL)
Orlando, Florida 32816

Eyal Sapir
CI Systems Inc.
5137 Clareton Drive, Suite 220
Agoura Hills, California 91301

Abstract. Measurements of modulation transfer function (MTF), particularly for staring imager systems, are affected by the position of the test target with respect to the rows and columns of the detector array. We demonstrate that random transparency targets of known spatial-frequency content allow shift-invariant MTF measurement in the visible, 3- to 5-μm, and 8- to 12-μm bands. Design criteria and verification procedures for the targets are presented.

Subject terms: modulation transfer function; sampling; aliasing; detector arrays; halftone transparencies; microlithography.

Optical Engineering 34(3), 860-868 (March 1995).

1 Introduction

A major problem encountered in measurement of MTF in sampled-image systems (such as staring or scanning imagers) is that the image modulation depth depends on the position of the deterministic target (typically a point source, line source, or bar target) with respect to the image sampling locations.[1–3] A random transparency test target of known spatial-frequency content allows measurement of a shift-invariant MTF because the information of the test target has random position with respect to the sampling sites. Random test targets have been used previously for MTF measurements of nonsampled systems such as camera lenses[4] and telescopes.[5]

An alternative technique, the scanning-knife-edge method,[6] has been developed to address the issue of shift variance in MTF measurement of imager systems that use focal-plane arrays (FPAs). A tilted knife edge is scanned across a column of the FPA. Our random-target method does not require mechanical scanning and tests the entire image plane at one time.

The random-target method creates random test patterns similar to those created using the laser-speckle method,[7] but on a broadband basis, without the use of laser radiation. This allows use of blackbody radiation for the source. This method tests both the FPA and the optics together, whereas the speckle MTF tests only the FPA.

Paper 04084 received Aug. 5, 1994; revised manuscript received Sep. 12, 1994; accepted for publication Sep. 13, 1994.

Proof-of-principle experiments were performed in the visible and in the infrared (IR). The random patterns were printed on different types of transparencies, fabricated either by xerographic exposure of a plastic film (for use in the visible and in the 3- to 5-μm band) or by electron-beam lithography involving a metal film on a ZnSe substrate (for use in both the 3- to 5-μm and the 8- to 12-μm bands).

2 Design of Random Transparencies

A computer algorithm to generate white-noise targets (i.e., random patterns) with the desired spatial-frequency properties was written by creating a vector of N random numbers, where N is the number of cells in a row of the target image. These N random numbers were generated using a parametric multiplicative linear congruential random generator that can produce a virtually infinite sequence of numbers.[8] This algorithm is a good random-number generator that will port to virtually all systems.[9] This vector is inserted into a loop to generate an array of $N \times N$ random numbers, resulting in an uncorrelated two-dimensional random pattern with a uniform bandlimited (up to the reciprocal of twice the pixel spacing) white-noise distribution (Fig. 1). Figure 2 is a schematic of the MTF measurement setup.

The uniformity of the background source is important to obtaining an accurate and repeatable measurement. The sources we used had less than 6% nonuniformity. In the visible experiments, we used an integrating sphere.[10] In the infrared, we used an extended-area blackbody source.

The random gray-level pattern is printed onto a transparency and placed in front of the uniform source, creating a

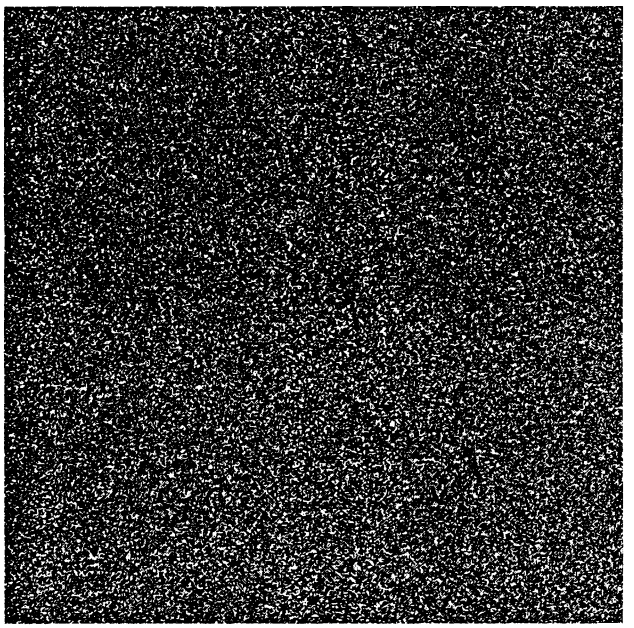

Fig. 1 Bandlimited white-noise random image.

two-dimensional radiance pattern. This creates an optical spatial-noise pattern with a known spatial power spectrum, $PSD_{in}(\xi)$, into the system, where ξ is the spatial frequency. The one-dimensional profile of the white-noise spectrum of the input image of Fig. 1 is shown in Fig. 3. We present a method in Sec. 4.3 for verifying the input power spectrum of transparency targets. This procedure calibrates any effects caused by the printing process, such as finite resolution or nonlinearities. This calibration produced only a small correction for the cases tested.

The output power spectral density, $PSD_{out}(\xi)$, is estimated by imaging the target through the optical system onto a charge-coupled device (CCD) FPA. The output image data are then captured by a frame grabber and processed to yield the output PSD as the $|FFT|^2$ of the output image data, averaged over the rows of the image. The input and output PSDs are related in the following manner:

$$PSD_{out}(\xi) = |H(\xi)|^2 PSD_{in}(\xi) \ , \tag{1}$$

where $|H(\xi)|$ is the system transfer function or MTF of the system.

The MTF measured using the random target of Fig. 1 is called the "continuous" MTF because it provides a continuous curve for all spatial frequencies of interest. In addition, another method was developed, called the "discrete" MTF, which allows us to measure the MTF at a number of discrete spatial frequencies as well as the spatial noise spectrum in the guardbands between these frequencies. This method was implemented by generating a filter with discrete narrowband components as shown in Fig. 4. This filter is then multiplied by the white-noise spectrum of Fig. 3 in the frequency domain, inverse Fourier transformed, and squared to obtain the desired discrete narrowband random image (Fig. 5). In creating the discrete filter, the triangles must be spaced symmetrically about zero frequency over the entire extent of the array, to avoid leakage when the fast Fourier transform (FFT) is taken. Note how the selected spatial frequencies in the filter

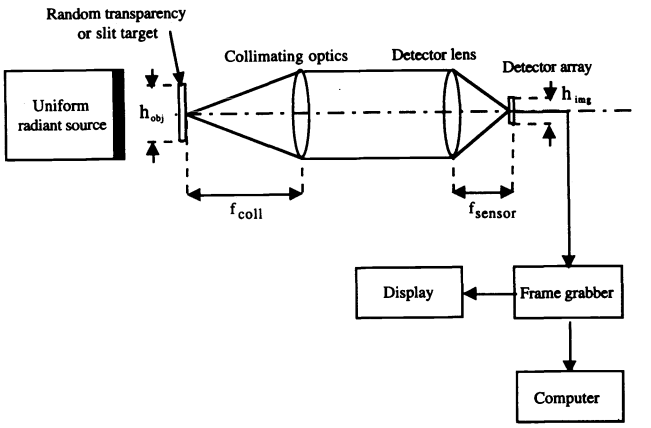

Fig. 2 Schematic of MTF measurement setup.

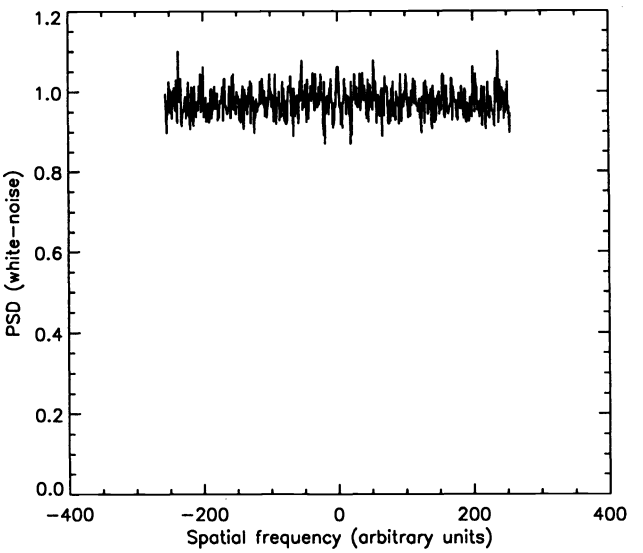

Fig. 3 $PSD_{input}(\xi)$ for white-noise spectral distribution.

appear in the image (i.e., a noticeable correlation between pixels exists), in comparison with the continuous case (Fig. 1), where no noticeable correlation between pixels exists.

A block diagram depicting the algorithm used to create both the white-noise and discrete transparencies is given in Fig. 6.

Use of the transparency-based targets avoids the linear falloff of $PSD_{in}(\xi)$ that would be present if laser speckle[7] targets were used. The attenuation of the PSD at the output of the system results solely from the system MTF. This constancy in the input PSD makes the MTF measurable to higher spatial frequencies than would be possible if PSD_{in} were bounded by an autocorrelation as in the case of laser speckle.

To optimize the pixel size of the random target to avoid aliasing, the limiting resolution of the system must be calculated. The pixel size of the random target imaged through the optics and falling onto the FPA is calculated by

$$l = \frac{h_{obj} M}{N} \quad [\mu m] \ , \tag{2}$$

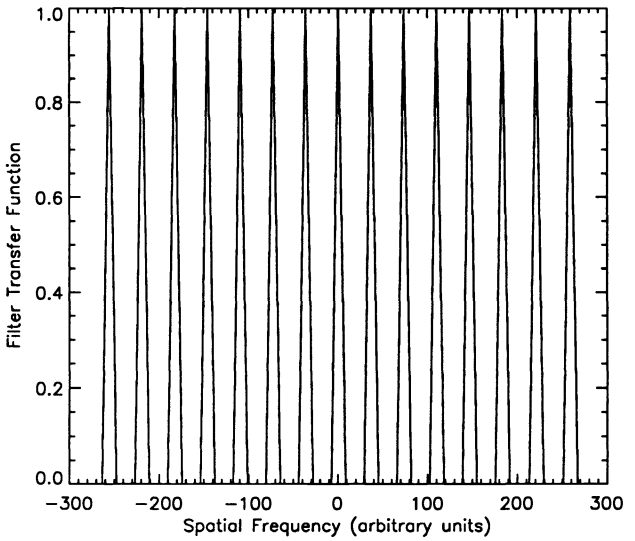

Fig. 4 Discrete filter transfer function.

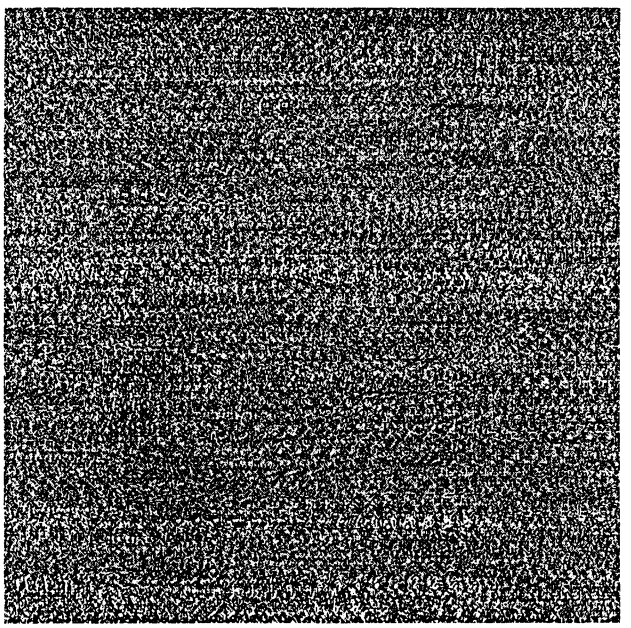

Fig. 5 Discrete narrowband random image.

where h_{obj} is the length of the random transparency, N is the number of cells in a row of the random target, and M is the measured transverse magnification of the optical system, which is given by

$$M = \frac{h_{img}}{h_{obj}} , \tag{3}$$

where h_{img} is the size of the FPA. The distance between the collimator and the detector lens should be as small as possible. This will minimize vignetting, allowing MTF measurement over the entire sensor field of view.

The maximum spatial frequency that can be obtained at the FPA is given by

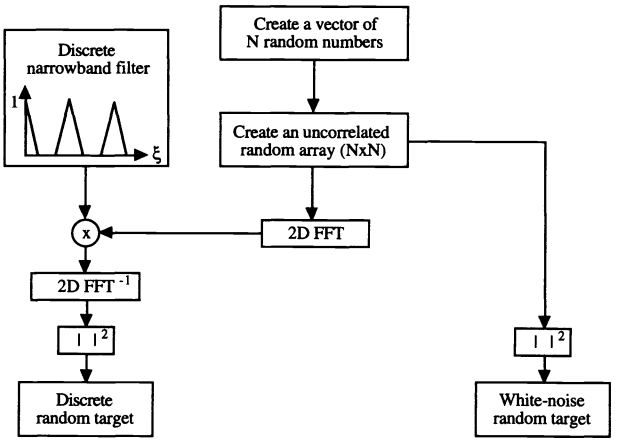

Fig. 6 Block diagram for the generation of random patterns.

$$\xi_{max} = \frac{1}{2l} \quad [\text{cycles/mm}] . \tag{4}$$

To avoid aliasing, ξ_{max} must be less than or equal to the spatial Nyquist frequency (ξ_{Ny}) of the FPA under test, which for detectors with center-to-center spacing d is given by

$$\xi_{Ny} = \frac{1}{2d} \quad [\text{cycles/mm}] . \tag{5}$$

The ultimate frequency resolution of the measurement is determined by the discrete Fourier transform (DFT) relationship, which requires the number of points in one domain to equal the number of points in the other domain. When a DFT is performed on a data set of length m, the Nyquist frequency appears at the $m/2$ component of the DFT output. A ratio[7] can be formed to evaluate the spatial frequency, ξ_i, which corresponds to the ith component as

$$\frac{\xi_{Ny}}{m/2} = \frac{\xi_i}{i} . \tag{6}$$

This associates frequencies between zero and ξ_{Ny} with DFT components from zero to the $m/2$ component.

3 Results—Visible Spectrum

A General Electric (GE) TN 2505 charge-injection device (CID) camera was tested using the system shown in Fig. 2. This camera responds to radiation of wavelength shorter than 1 μm, and has a standard RS170 analog video output. The data were digitized to 8 bits with a frame grabber. The random target was printed onto standard overhead transparency material using a laser printer.

The continuous MTF, discrete MTF, and spatial-noise amplitude spectrum were measured in the horizontal direction. The standard line-spread function method was also used to facilitate a comparison. The detector array for this camera had 377 (horizontal) pixels, with a pixel pitch $d = 23.4$ μm, yielding $h_{img} = 8.82$ mm. The physical parameters of the measurement system were

$$f_{sensor} = 50 \text{ mm} ,$$

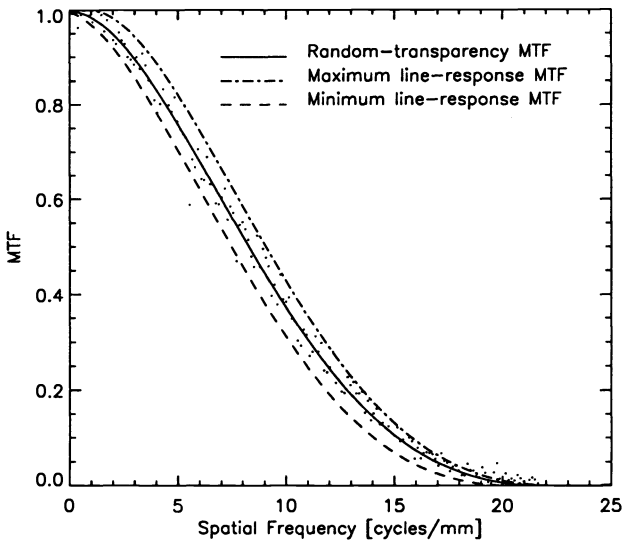

Fig. 7 Random-transparency MTF (polynomial fit—solid line); maximum line-response MTF (dot-dashed line); minimum line-response MTF (dashed line) for the visible CID camera system. The discrete points are the raw data for the random-transparency MTF.

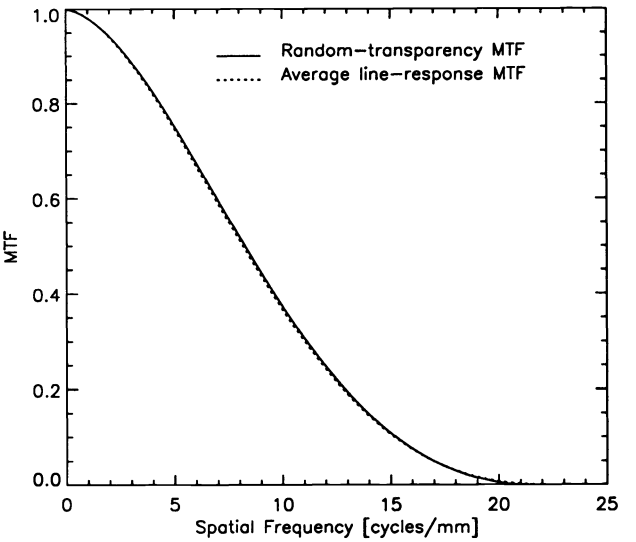

Fig. 8 Continuous random MTF (solid line); average-line response MTF (dotted line) for the visible CID camera system.

$f_{\text{coll}} = 17.5$ in. $= 444.5$ mm ,

$L = 110$ mm ,

$N = 512$ pixels ,

where L is the length of the printed pattern. A length $h_{\text{obj}} = 81$ mm out of the 110 mm of L was imaged onto the FPA, resulting in $N = 377$ pixels. Given the system magnification, the system parameters are calculated as follows:

$l = 23.4$ μm from Eq. (2) ,

$M = 0.109$ from Eq. (3) ,

$\xi_{\max} = 21.4$ cycles/mm from Eq. (4) ,

$\xi_{\text{Ny}} = 21.5$ cycles/mm from Eq. (5) .

3.1 *Continuous MTF*

The MTF of the system was measured in the usual way for comparison, by applying a line source at the input of the system of width $w = 50$ μm. This slit target is carefully oriented parallel to the columns of the sensor array, and was moved relative to the sampling sensor grid until maximum and minimum signals were obtained at the sensor output. The system's response to the line source is the line-spread function (LSF). The absolute value of the one-dimensional FFT of the LSF was calculated, averaged over the rows of the image, and divided by the FFT of the finite width of the line source to correct for the nonwhite input spectrum (a sinc function), and normalized to one at dc. The maximum line-response MTF is obtained when the line-source image is centered on the photosites. The minimum line-response MTF is obtained when the line-source image is centered between the photosites.

The results from the LSF method and the random-transparency method are compared in Fig. 7. The random-transparency MTF is calculated from the output PSD according to Eq. (1). The raw data points are shown along with a fourth-order polynomial fit given by the solid curve. The polynomial-fit procedure is used for presentation of all random-target MTF curves in this paper. The amount of variation seen in the raw data in Fig. 7 is typical of all data sets. The maximum and minimum LSF-derived MTFs are shown as the dot-dashed and dashed curves respectively. Note that the random-transparency MTF curve lies between the maximum and minimum line-response MTF curves. Individual data points are the result of a particular spatial-frequency component in the image. This component has a random position with respect to the photosite locations. The data points thus generally fall between the maximum and minimum LSF-derived MTF curves.

The average MTF was also measured using the LSF method. The line source was moved randomly, and 15 LSF-derived MTFs were calculated and averaged. The comparison between the random-tansparency MTF (solid curve) and the average LSF-derived MTF (dotted curve) is shown in Fig. 8. Their excellent agreement is consistent with the analysis of Park et al.,[2] where a shift-invariant MTF is calculated as the average over all possible test-target positions.

The repeatability of the random-transparency method was measured by making in-plane translations of the transparency and comparing the resulting MTFs. The variation in MTF was less than 2%. The random-transparency method is thus demonstrated to be shift invariant. This shift invariance relaxes alignment requirements in the test procedure, as compared to the LSF method, in which the test operator must find the maximum and minimum LSF responses.

3.2 *Discrete MTF and Spatial Noise Spectrum*

Using the discrete target of Fig. 4, the discrete MTF and spatial-noise amplitude spectrum shown in Fig. 9 were measured. The filtering effect of the MTF is seen by the decrease in the heights of the triangle peaks.

The spatial-noise amplitude spectrum of the system was independently measured by taking the |FFT| of the array data

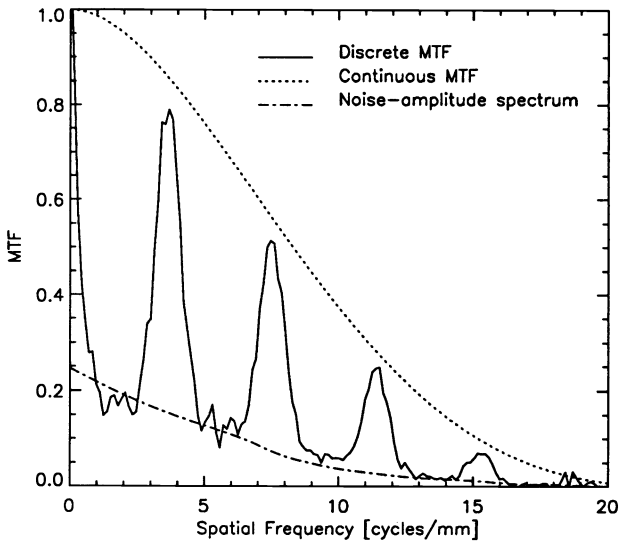

Fig. 9 Discrete MTF (solid curve); continuous random-transparency MTF (dotted line); noise-amplitude spectrum (dashed line).

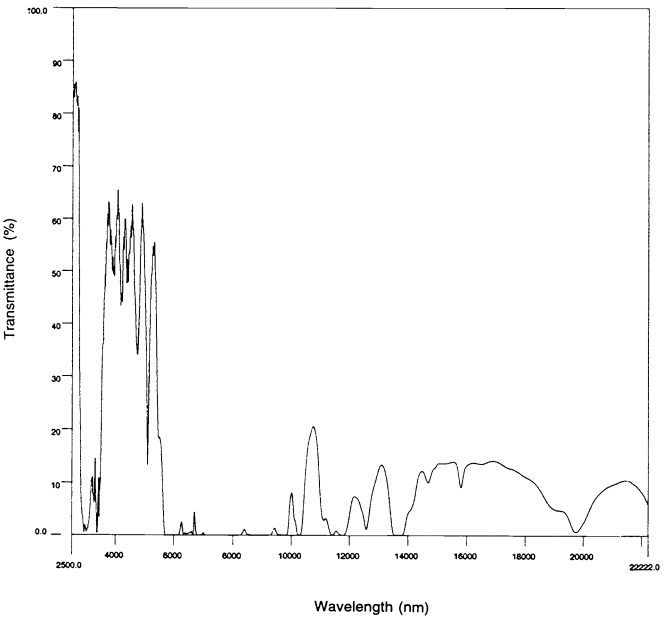

Fig. 10 Spectral properties of the ortho-film transparency.

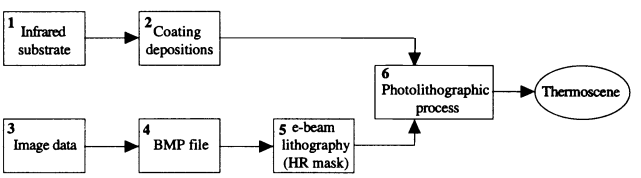

Fig. 11 Block diagram of the manufacturing process of the random thermoscene.

(averaged over the rows) when flux was incident on the array at the same average value as for the target image. The results of the continuous and discrete methods, and the spatial noise-amplitude spectrum, are superimposed in Fig. 9; note how the continuous curve fits the height of each of the discrete measurements, and how the noise-amplitude spectrum matches the levels in the guardbands between the triangles. The discrete method allows us to measure both MTF and spatial noise as a discrete function of spatial frequency, which can be used to calculate a spatial-frequency-dependent signal-to-noise ratio.

4 Results—Infrared Spectrum

Transmission regions of most IR optical materials differ from those of visible materials; thus visible transparencies do not have necessarily good transmission in the infrared. To perform the MTF measurements in the IR spectrum, the random target data must be transferred to an IR substrate with the desired transmission properties. An infrared halftone transparency, or thermoscene,[11–13] has been developed to simulate a two-dimensional random pattern in the IR atmospheric windows (3 to 5 μm and 8 to 12 μm). The fabrication of these thermoscenes for the 8- to 12-μm band is expensive because of materials and lithographic costs. However if the MTF testing is performed only in the 3- to 5-μm band, a plastic transparency (ortho-film), can be used as the target substrate, considerably reducing the system cost. The fabrication of both the transparencies and the random thermoscene are now explained.

4.1 *Generation of the Ortho-Film Transparency*

The $N \times N$ random image with 256 different gray scales created by the computer algorithm is printed using a high-resolution (1200 dpi) printer. The image is then photographically reduced to the required size on a Kodalith ortho-film 2556, type 3 (ESTAR base) from Kodak. The spectral properties of the clear areas of the ortho-film transparency are shown in Fig. 10. As we can see, the transparency transmits about 55% in the 3- to 5-μm region, but the average transmission in the 8- to 12-μm region is around 5%. Transmission in the visible portion of the spectrum was above 95%. The opaque regions of the ortho-film transparency showed negligible transmission. This transparency can thus be used to test both visible and 3- to 5-μm systems.

4.2 *Generation of the ZnSe Transparency*

In the 8- to 12-μm band, the ortho-film transparency must be replaced by a random thermoscene made of a chrome deposition on a zinc selenide (ZnSe) substrate. This is also usable in the 3- to 5-μm band. Microlithographic processes enable us to produce square apertures of various sizes on a two-dimensional matrix to achieve the desired random pattern. To avoid diffraction-induced nonlinearities of transmittance, the minimum aperture size must be four times the light wavelength.[14]

Figure 11 is a block diagram of the random-thermoscene manufacturing process. The initial processes are independent of each other and can be carried out separately until the photolithographic step. The steps in Fig. 11 are:

- *Step 1.* A ZnSe window with a diameter of 50.8 mm is used as the infrared substrate. We limit the active area of the window to 48.8 mm to leave a 1-mm-wide rim, which is adequate for coating fixtures and processing geometry. The overall size of the random pattern is then a square of 34.5×34.5 mm.

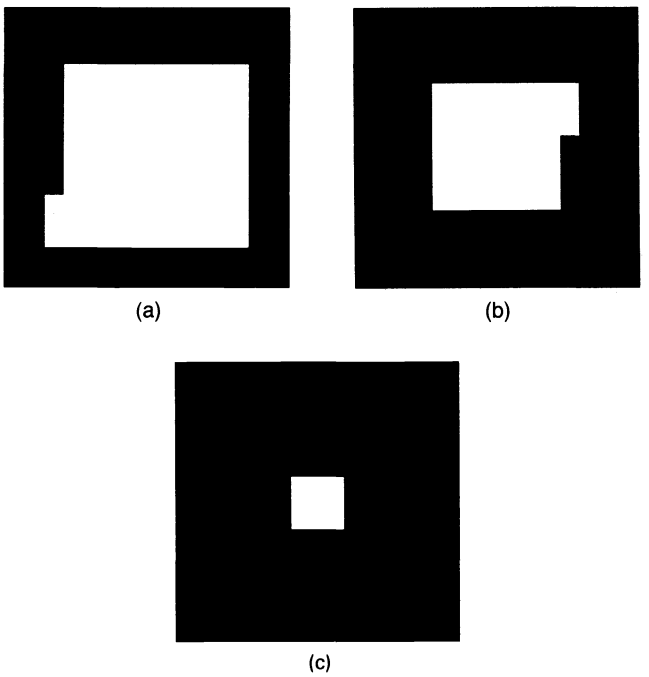

Fig. 12 Examples of pixels with different gray levels showing spiral structure: (a) high-transmission pixel, (b) medium-transmission pixel, and (c) low-transmission pixel.

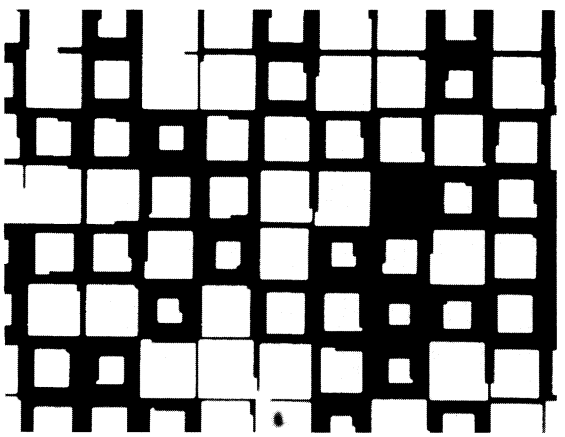

Fig. 13 Magnification of different gray levels on the HR mask. The period of the pixels is 46 μm.

- *Step 2.* The deposition on the ZnSe substrate consists of two different layers deposited on one side of the window. The first layer consists of 50 nm of silicon oxide (SiO_2) to protect the ZnSe substrate from the chemical etching when the photolithographic process is applied. The second layer consists of 80 nm of chrome, which prevents any transmittance in the opaque regions.
- *Step 3.* A single file consists of $N \times N$ bytes, where each byte equals one pixel in the original image. A byte is equal to the intensity of its corresponding pixel on a gray scale of 0 to 255 (0 = white, 255 = black or vice versa). The bytes are stored in the file in a continuous string, with the first byte representing the bottom left pixel and each following byte representing the next pixel to the right until the end of the row, at which point the next pixel is the leftmost pixel of the next row up.
- *Step 4.* The image data are stored to a bit-map (BMP) file.
- *Step 5.* Electron-beam lithography is used to generate the random pattern on a high-resolution (HR) photomask directly from the computer data. A focused electron beam exposes a radiation-sensitive resist layer on top of the chrome producing microstructural changes, such as crosslinking, that enables the pattern to be developed. The required number of gray levels in a spiral pattern seen in Fig. 12 is obtained by dividing each pixel into subpixels. The area of the subpixels is determined by

$$\text{subpixel area} = \frac{\text{maximum aperture area} - \text{minimum aperture area}}{\text{dynamic range} - 2}, \tag{7}$$

where the subtraction of 2 in the denominator corresponds to the two first gray levels (i.e., the totally opaque pixel and clear-aperture pixel). Figure 13 shows a magnified image of the mask. The spatial resolution using this technique is 1 ± 0.1 μm.

- *Step 6.* In this stage the two independent processes of Fig. 11 combine to produce the final product (i.e., the random thermoscene) using a photolithographic process, which replicates the pattern from the photomask to the desired IR substrate. The pattern cannot be generated directly on the IR substrate, because of the cost involved in deviating from standard substrates.

The photolithographic technique is shown in Fig. 14. The IR substrate to be patterned is coated with a thin (≤ 1 μm) layer of a photoresist material by a standard liquid-spinning technique. It is then illuminated with a collimated parallel beam of light from a UV source (200 to 450 nm), through the aligned-beam chrome mask. The chrome mask is pressed against the infrared substrate (contact printing). Depending on the nature of the photoresist used, it hardens (negative photoresist) or softens (positive photoresist) on being exposed to the UV radiation through the transparent regions of

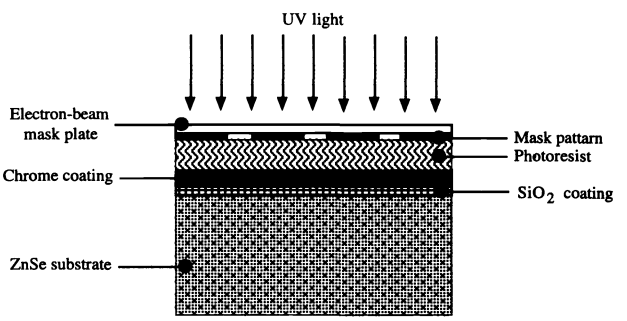

Fig. 14 Coating depositions and photolithographic process.

the mask. The hard regions are fixed to become resistant to chemical etching in the appropriate solvent or developer. Thus, depending on the nature of the photoresist used, a positive or negative image of the chrome mask can be created in the required IR substrate. The resolution using this technique with 400-nm exposing radiation is 3 ± 0.25 μm.

4.3 *Continuous MTF—3- to 5-μm Band*

The procedure for testing the MTF using random IR transparencies utilizes the experimental setup shown in Fig. 2 and an extended-area blackbody as the uniform source.

The measurement in the 3- to 5-μm spectral range is performed by imaging the random test pattern onto a platinum silicide (PtSi) Schottky-barrier CCD (Mitsubishi IR-5120A). The array consists of 512×512 detector elements, with a pixel pitch of 26 μm (horizontal) $\times$ 20 μm (vertical). The effective length of the random pattern imaged on the CCD FPA was $h_{obj} = 23.6$ mm.

The optical system is optimized when the Nyquist frequency of the FPA and the maximum target spatial frequency are equal. To achieve optimization, the effective size of the random pattern $h_{obj} = 23.6$ mm must contain 512 resolution elements (pixels), and the total size of the random pattern must be composed of 750 pixels (i.e., the size of the random pattern is a square of 34.5 $\times$ 34.5 mm). A film transparency was generated having 256 gray levels using the above specifications.

For the design of the random thermoscene, the maximum aperture spacing (pixel size) is (34.5 mm)/750 = 46 μm with a minimum hole size of 16 μm (approximately 4 times the wavelength[14]). Then the requirement of 8-bit dynamic range from the thermoscene (256 gray levels) implies a linear increment for each gray level (subpixel area) that, according to Eq. (7), is $(46^2 - 16^2)/254 = 7.3$ μm^2. This corresponds to a resolution element (subpixel size) of 2.7 μm.

The 3- to 5-μm infrared system is evaluated in the same form as the visible system:

l = 46 μm from Eq. (2),

M = 0.564 from Eq. (3),

ξ_{max} = 19.3 cycles/mm from Eq. (4),

ξ_{Ny} = 19.2 cycles/mm from Eq. (5).

The maximum and minimum line responses using the LSF method are compared with the results from the film transparency in Fig. 15 for the 3- to 5-μm spectral region. The LSF was measured by locating a slit target of width $w = 50$ μm to the focal plane of the collimation lens in Fig. 2. The continuous MTFs measured using both the film transparency and the thermoscene in the 3- to 5-μm band are compared in Fig. 16.

The MTF curve measured using the thermoscene is lower than that evaluated using the transparency because of defects in the photolithographic deposition process. The substrate is covered with spots of chrome, and apertures that should be transparent are covered by a thin layer of chrome as shown in Fig. 17. We postulate that these fabrication defects cause a rolling off of the $PSD_{in}(\xi)$, as compared to either the mask itself (Fig. 13) or the film transparency.

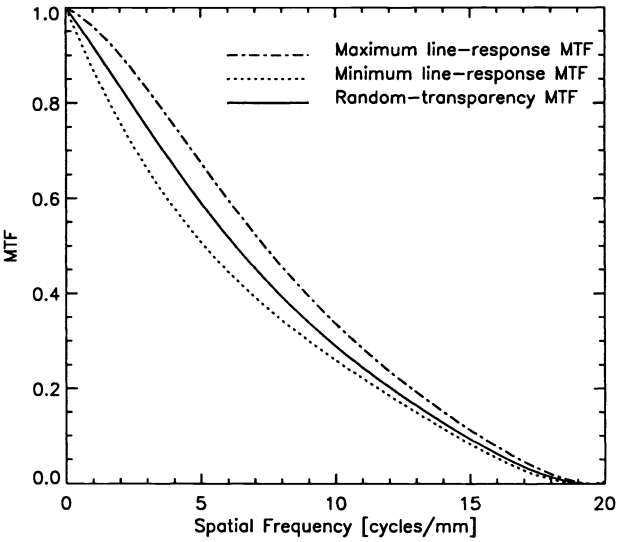

Fig. 15 Random MTF evaluated using a film transparency (solid curve), the maximum line-response MTF (dashed line), and the minimum line-response MTF (dotted line) for the 3- to 5-μm infrared spectrum.

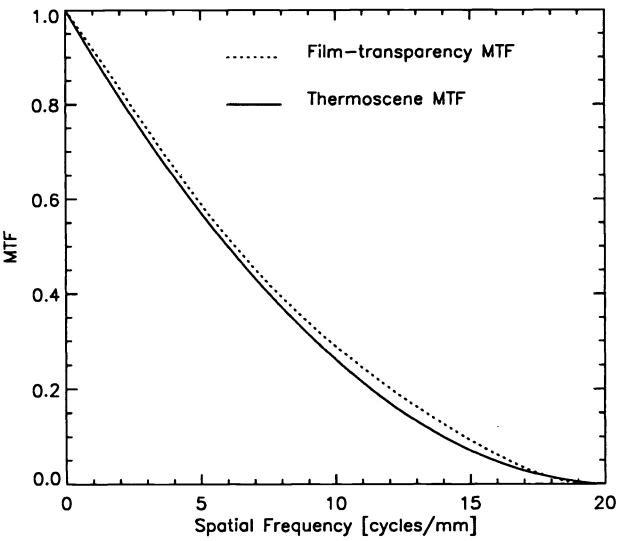

Fig. 16 Thermoscene MTF curve (solid line); film-transparency MTF curve (dotted line).

A test procedure to characterize the input target PSD for thermoscenes is as follows. First, a small portion of the random pattern is magnified and imaged through a microscope onto a visible-light CCD array (Pulnix TM-7CN). The image is then captured by a frame grabber and processed. The image is an array of 512×480 pixels. The pixel values are thresholded (i.e., the pixel values less or equal to 128 are set to zero, and those greater than 128 are set to 255) to obtain a binary pattern suitable for area measurement. The resulting image data are averaged over successive 32×16-pixel regions, corresponding to the thermoscene pixels. A value from 0 to 255 is assigned to each region. We repeat these steps 16 times for 16 horizontal contiguous regions. The sixteen images are put together in a string obtaining an array of 512×16 pixels. Finally, the one-dimensional $|FFT|^2$ of this array is

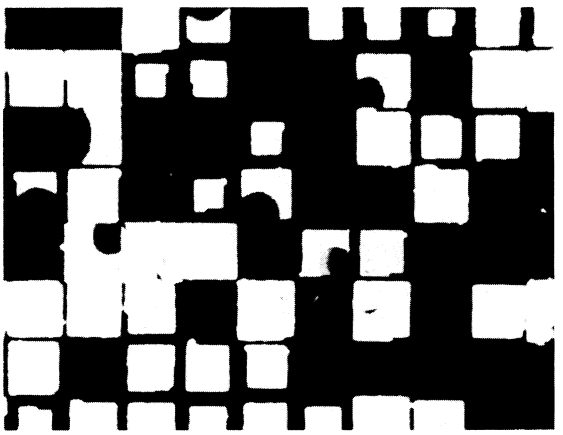

Fig. 17 Magnification of different gray levels of the random thermoscene. The period of the pixels is 46 μm.

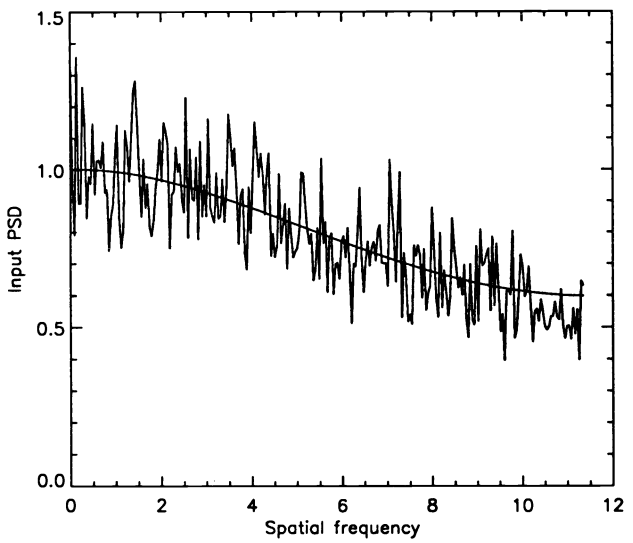

Fig. 18 Attenuated input spectral density distribution and polynomial fit of fourth order.

calculated and averaged over successive rows. The result is a nonwhite PSD, which is shown in Fig. 18. A polynomial fit of fourth order of the input spectrum was evaluated to be used in Eq. (1) for the calculation of the MTF. This calibration procedure was applied to the random thermoscene MTF curve of Fig. 16. The result is shown in Fig. 19, which shows that this correction has produced excellent agreement between the two types of random transparencies.

4.4 *Continuous MTF—8- to 12-μm Band*

To demonstrate the random MTF method in the 8- to 12-μm spectral range, an infrared scanner Magnavox IR-18 with mercury cadmium telluride (HgCdTe) SPRITE detectors and an afocal telescope was tested. The video output is RS-170 compatible. The test setup of this system is shown in Fig. 2.

The specifications of the imager without the telescope interface are $f_{\text{sensor}} = 36.4$ mm; $f/2.5$; FOV $= 38 \times 25.5$ deg; horizontal instantaneous field of view (HIFOV) 1.7 mrad; and 400 horizontal lines per frame.

Taking the product between the HIFOV and f_{sensor}, the pixel size in the horizontal direction is 61.9 μm. The resolution of the imager in the same direction (i.e., total number of pixels) is also found by dividing the HFOV by the HIFOV, resulting in $N = 390$ pixels. Therefore, the effective size of the detector array in that direction is $h_{\text{img}} = 24.14$ mm.

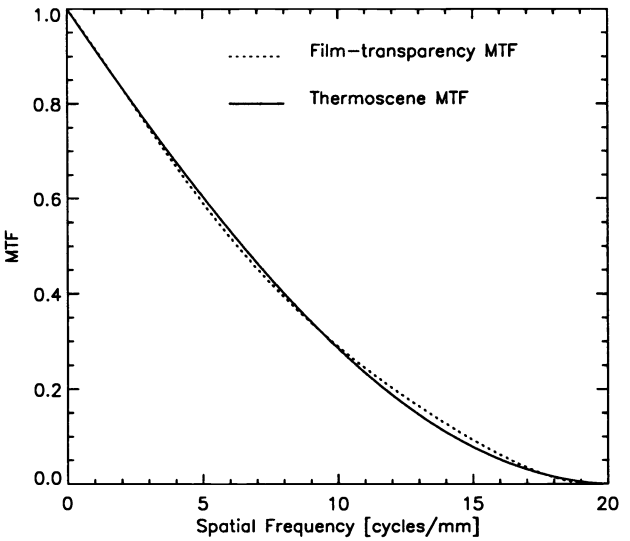

Fig. 19 Corrected thermoscene MTF curve (solid line), film-transparency MTF curve (dotted line), both measured in the 3- to 5-μm band.

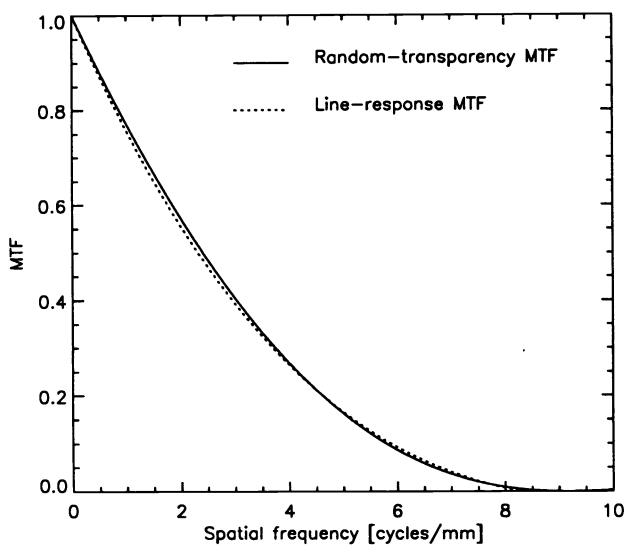

Fig. 20 Continuous random MTF curve (solid line), line-response MTF (dotted line) for the 8- to 12-μm system.

With the afocal telescope in place, the system focal length of the system ranges between 65.52 and 164.34 mm for the wide field of view (WFOV) and narrow field of view (NFOV) respectively. The dimension h_{obj} was measured to be 8 mm for the NFOV and 20 mm for the WFOV. Therefore, when the telescope is used, an adjustable magnification between 1.2 and 3 can be achieved using Eq. (3) for the WFOV and NFOV respectively. Because of this flexibility, the magnification of the system is set in such a way that the same design used to develop the ZnSe random thermoscene for the 3- to 5-μm band can be used to measure the MTF of the 8- to 12-μm system.

The size of the thermoscene designed for the 3- to 5-μm system is 34.5 mm, with 750 pixels. The required resolution of the 8- to 12-μm system is 390 pixels; therefore, the portion of the random target imaged through the optics onto the detector must have a length of $h_{obj} = 17.9$ mm. Hence, by setting a magnification of $M = 1.34$ we prevent aliasing. The line response using the LSF method is compared with the random method in Fig. 20 for the 8- to 12-μm band. In this case, the line-response MTF is equivalent to the average MTF as a result of the scanning mechanism inherent in the 8- to 12-μm system. The MTF curve using the random thermoscene was evaluated taking into account the actual input spectrum for the system in Fig. 18 using Eq. (1).

5 Conclusions

A shift-invariant measurement technique for the MTF, based on random transparency targets of known spatial-frequency content, has been demonstrated in the visible, 3- to 5-μm, and 8- to 12-μm bands. The method can be used with plastic transparencies for the visible and the 3- to 5-μm band, and with lithographic halftone transparencies for the 3- to 5-μm and 8- to 12-μm bands. This method produces results that agree well with the position-averaged line-response MTF, and has relaxed alignment tolerances compared to methods that employ deterministic targets. This technique is used to test complete image systems, consisting of a sampled-image receiver and associated optics. Both white-noise and discrete-frequency targets are possible.

Acknowledgments

We would like to express our appreciation to Dr. Karl Guenther from CREOL, and Dr. Ernest B. Tley of the Friedrich-Schiller Universität Jena, Institut fur Angewandte Physik, in Germany, for the fabrication of the random ZnSe thermoscene. We thank CI Systems Inc. for participating in and sponsoring this research.

References

1. W. Wittenstein, J. C. Fontanella, A. R. Newbery, and J. Baars, "The definition of OTF and the measurement of aliasing for sampled image systems," *Opt. Acta* **29,** 41–50 (1982).
2. S. K. Park, R. Schowengerdt, and M. Kaczynsky, "Modulation transfer function analysis for sampled image systems," *Appl. Opt.* **23,** 2572–2582 (1984).
3. S. E. Reichenbach, S. K. Park, and R. Narayanswamy, "Characterizing digital image acquisition devices," *Opt. Eng.* **30**(2), 170–177 (1991).
4. H. Kubota and H. Ohzu, "Method of measurement of response function by means of a random chart," *J. Opt. Soc. Am.* **47**(7),666–667 (1957).
5. C. Aime, "Measurement of averaged squared modulus of atmospheric lens modulation transfer function," *J. Opt. Soc. Am.* **64**(8), 1129–1132 (1974).
6. Wong Hon-Sum, "Effect of knife-edge skew on MTF measurements of CCD imagers employing a scanning knife edge," *Opt. Eng.* **30**(9), 1394–1398 (1991).
7. M. Sensiper, G. D. Boreman, A. D. Ducharme, and D. R. Snyder, "MTF testing of detector arrays using narrow-band laser speckle," *Opt. Eng.* **32**(2), 395–400 (1993).
8. Lehmer, D. H., "Mathematical methods in large-scale computing units," *Annu. Comput. Lab. Harvard Univ.* **26,** 141–146 (1951).
9. S. K. Park and K. W. Miller, "Random numbers generators: Good ones are hard to find," *Commun. ACM* **31**(10), 1192–1201 (1988).
10. A. D. Ducharme, G. D. Boreman, A. Daniels, and E. B. Grann, "Low cost integrating sphere for uniform illumination," *IEEE Trans. Educ.* submitted for publication.
11. S. Ghilai, U. Gera, D. Cabib, A. Lapin, and Y. Liran, "Infrared transparencies (thermoscenes) for simulation of infrared scenes as a tool to improve FLIR testing," *Proc. SPIE* **819,** 80–86 (1987).
12. D. Cabib, J. Eliason, S. Guilai, and R. Bracha, "Accurate infrared scene simulation by means of microlithographically deposited substrate," *Proc. SPIE* **1762,** 376–384 (1992).
13. A. Daniels, "The thermoscene—a basic component of infrared simulation," MSc Thesis, Univ. of Tel-Aviv (1989).
14. A. Daniels, G. D. Boreman, and E. Sapir, "Diffraction effects in infrared halftone transparencies," *Infrared Phys. and Technol.* **36**(2) (1995).

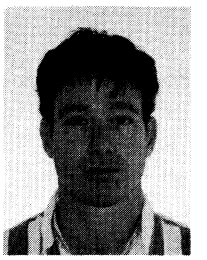

Arnold Daniels received a BSc in electrical engineering from the Autonomous University of Mexico (UNAM) in 1984 and a BSc in electrical engineering from the Israel Institute of Technology (Technion) in 1987. He received an MSc in electrical engineering from the University of Tel-Aviv in 1989. He worked as an optical engineer for CI Systems (Israel) Ltd., before joining the Center for Research and Education in Optics and Lasers (CREOL) at the University of Central Florida, where he received a PhD in electrical engineering in 1994.

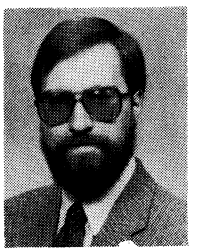

Glenn D. Boreman is an associate professor of electrical engineering in the Center for Research and Education in Optics and Lasers (CREOL) at the University of Central Florida. He received a BS from the Institute of Optics, University of Rochester, and a PhD from the Optical Sciences Center, University of Arizona. He has held visiting research positions at IT&T, Texas Instruments, U.S. Army Night Vision Lab, and McDonnell Douglas. Dr. Boreman serves as topical editor for *Applied Optics* in the areas of radiometry and detectors and is past president of the Florida Optical Society.

Alfred D. Ducharme received the BSEE degree from the University of Lowell, now known as the University of Massachusetts at Lowell, in 1990, and the MSEE and PhD degrees from the University of Central Florida in 1992, and 1994, respectively, while working as a graduate research assistant at the Center for Research and Education in Optics and Lasers. His research interests include statistical optics and laser speckle.

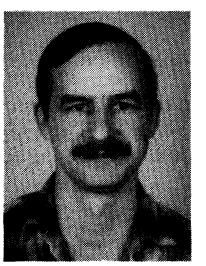

Eyal Sapir received the BS and MS degrees in electrical engineering from the Israel Institute of Technology (Technion) in 1980 and 1984, respectively. He has been working at CI Systems (Israel) Ltd. since 1980. He is the product manager of the FLIR test equipment group in the company.